

# Quantized monopole nonlinear Hall current from Chiral asymmetry

Nikolai Peshcherenko,<sup>1</sup> Claudia Felser,<sup>1</sup> and Yang Zhang<sup>2,3</sup>

<sup>1</sup>Max Planck Institute for Chemical Physics of Solids, 01187, Dresden, Germany

<sup>2</sup>Department of Physics and Astronomy, University of Tennessee, Knoxville, TN 37996, USA

<sup>3</sup>Min H. Kao Department of Electrical Engineering and Computer Science, University of Tennessee, Knoxville, Tennessee 37996, USA

We propose a topological probe for detecting chirality imbalance in time reversal invariant Weyl and Dirac semimetals via nonlinear Hall response. The chiral anomaly effect, occurring in parallel electric and magnetic fields, causes a energy shift between Weyl cones of different chirality, which leads to chirally asymmetric intra-node relaxation. The net nonlinear Hall current is thus quantized, and determined by the sum of monopole charge weighted by the transport relaxation time. Our theory directly applies to chiral Weyl semimetals even without a magnetic field. Additionally, besides DC transport probes, we anticipate that nonlinear circular dichroism measurements could detect chiral asymmetry-induced currents.

*Introduction.* In Weyl semimetals (WSM), the conduction and valence bands exhibit a linear crossing in the three-dimensional (3D) momentum space, occurring near the Fermi energy at nodal points referred to as Weyl points. The Weyl points act as sources or sinks of the Berry curvature, giving rise to distinctive topological characteristics crucial for experimentally detecting WSM. Two most well-established features encompass Fermi arcs in spectroscopic experiments, and chiral anomalies in transport experiments. Chiral anomaly effect was predicted to occur under parallel electric and magnetic fields long ago [1], and the widely discussed experimental proof has been the negative longitudinal magnetoresistance, both in Weyl [2–6] and Dirac semimetals [7–13].

However, it was later realized that the negative longitudinal magnetoresistance could not serve as a unambiguous evidence of chiral anomaly. There are other completely topology-unrelated non-isotropic contributions present, e.g., ‘current jetting’ effect [14–17]. Moreover, the current jetting effect is especially strong in topological semimetals, including Dirac and Weyl semimetals. The direct observation of Berry curvature-related anomalous velocity in longitudinal transport phenomena remains challenging. Therefore, it is essential to explore different physical setups for a more robust investigation of chiral anomaly physics.

In this work, we propose a topological probe of chiral anomaly, where chirality imbalance of Weyl nodes are directly associated with net Hall current. In time-reversal (TR)-invariant systems, the non-vanishing Berry curvature induced Hall current could only be non-linear [18]. The crucial ingredients of our approach are the combination of anomalous velocity and shifted Fermi surface due to finite electric field. Since the Fermi surface shift itself is proportional to intra node momentum relaxation time, we prove that the result for non-linear Hall conductivity in Weyl semimetals is given by the sum of Berry curvature flux-proportional terms, weighted by momentum relaxation times within each Weyl node. Thus, the observation of the nonlinear Hall current requires an explicit chiral symmetry breaking, under chiral anomaly or

intrinsic mirror symmetry breaking [19–22].

In the extreme chiral limit, where remote Weyl nodes have vanishing relaxation times, the nonlinear Hall current arises solely from the Weyl monopoles near the Fermi level, as a simplification of Berry curvature dipole mechanism. The nonlinear Hall effect from dipole moment of Berry curvature [18] requires a certain degree of electron’s spectrum anisotropy (e.g., tilted Weyl nodes [23, 24]), while the monopole nonlinear Hall effect from chiral asymmetry allows one to observe a topological monopole contribution not limited by extra anisotropy requirement. We further demonstrate that chiral asymmetry induced nonlinear Hall current could be also observed via nonlinear circular dichroism measurements. Calculations are made both within semiclassical Boltzmann equation, and the fully quantum approach using Kubo formula. Moreover, all of the physics discussed above applies to Dirac semimetals.

*Semiclassical description.* We start our consideration with semiclassical description of non-linear charge current  $\mathbf{j}$  in topological Weyl semimetals. The low energy electronic properties of these systems are well captured by the Weyl Hamiltonian

$$H = \eta v_F \boldsymbol{\sigma} \cdot \mathbf{k}, \quad (1)$$

so that electronic states with momentum  $\mathbf{k}$  possess non-trivial Berry curvature  $\boldsymbol{\Omega}_\eta(\mathbf{k})$ , where  $\eta = \pm 1$  stands for node’s chirality.

The general semiclassical expression for  $\mathbf{j}$  is given by

$$\mathbf{j} = e \sum_{\eta} \sum_{\mathbf{k}} \mathbf{v}_\eta f_\eta(\mathbf{k}), \quad \mathbf{v}_\eta = \nabla_{\mathbf{k}} \varepsilon_\eta(\mathbf{k}) + \boldsymbol{\Omega}_\eta \times \dot{\mathbf{k}},$$

$$\dot{\mathbf{k}} = e\mathbf{E} + \frac{e}{c} \mathbf{v} \times \mathbf{B}, \quad (2)$$

where electron velocity  $\mathbf{v}_\eta$  is given by a sum of group velocity  $\nabla_{\mathbf{k}} \varepsilon_\eta(\mathbf{k}) = \eta v_F \mathbf{k}/|\mathbf{k}|$  and anomalous velocity contribution  $\boldsymbol{\Omega}_\eta \times \dot{\mathbf{k}}$ . The system is subject to electric and magnetic fields. For calculation of distribution function  $f_\eta$  we employ Boltzmann equation:

$$-i\omega f_\eta + e\mathbf{E}(\omega) \cdot \nabla_{\mathbf{k}} f_\eta = -\frac{\delta f_\eta}{\tau_\eta}, \quad (3)$$

where  $\tau_\eta$  is node-dependent intranode momentum relaxation time,  $\delta f_\eta$  describes deviation from equilibrium and  $\mathbf{E}(\omega)$  is Fourier image of time-dependent electric field  $\mathbf{E}(t)$ . For  $\delta f_\eta$  we then find

$$\delta f_\eta(\omega) = -\frac{e\mathbf{E}(\omega)\nabla_{\mathbf{k}}f_0}{-i\omega + 1/\tau_\eta} \quad (4)$$

so that for Hall current  $\mathbf{j}_H(\omega_j)$  we arrive at

$$\mathbf{j}_H(\omega_j) = -e^2 \int \frac{d\omega}{2\pi} \sum_{\eta} \sum_{\mathbf{k}} \boldsymbol{\Omega}_\eta \times \mathbf{E}(\omega_j - \omega) \frac{e\mathbf{E}(\omega)\nabla_{\mathbf{k}}f_0}{-i\omega + 1/\tau_\eta}, \quad (5)$$

where Hall current frequency  $\omega_j$  is either  $\omega_j = 0$  or  $\omega_j = 2\omega_0$ , with  $\omega_0$  being the electric field frequency. Note that in Eq. (5), we deliberately dismissed linear in  $\mathbf{E}$  contribution due to its proportionality to net Berry curvature  $\sum_{\eta} \boldsymbol{\Omega}_\eta$ , which is known to vanish in TR invariant systems. The second order response in Eq. (5) accounts both for anomalous velocity and for the shift of Fermi surface in the course of applied electric field  $\mathbf{E}$  (see Fig. 1a). In the extreme driving limit where  $\tau_\eta \gg \tau_{-\eta}$ , we have a net nonlinear dc current from Berry curvature monopole, as a reduction of so-called 'Berry curvature dipole' [18] nonlinear Hall current. In our setup, it is crucial to have a node-dependent relaxation time  $\tau_\eta$  as a probe of chirality imbalance. Note also that in Eq. (5), we explicitly neglected  $B$ -proportional Lorentz force part [25] from Eq. (2), since it is a higher order correction from the Weyl nodes tilting.

Then for Weyl nodes with  $\boldsymbol{\Omega}_\eta(\mathbf{k}) = \eta\mathbf{k}/2|\mathbf{k}|^3$ , we finally arrive at the following expression for Hall current  $j_{H\alpha}$ :

$$\begin{aligned} j_{H\alpha}(\omega_j) &= e^3 \varepsilon_{\alpha\beta\gamma} \int \frac{d\omega}{2\pi} \sum_{\mathbf{k}} \Omega_{\beta} E_{\gamma}(\omega_j - \omega) E_{\delta}(\omega) n_{\delta} \cdot \\ &\quad \cdot \delta(|\mathbf{k}| - k_{F,\eta}) \frac{\tau_{\eta}(\varepsilon)}{1 - i\omega\tau_{\eta}(\varepsilon)} = \\ &= \frac{e^3}{3} \varepsilon_{\alpha\beta\gamma} \int \frac{d\omega}{2\pi} E_{\beta}(\omega) E_{\gamma}(\omega_j - \omega) \sum_{\eta} \frac{\tau_{\eta}(\mu_{\eta})}{1 - i\omega\tau_{\eta}(\mu_{\eta})} \cdot \\ &\quad \cdot \int \frac{\boldsymbol{\Omega}_{\eta} \cdot d\mathbf{k}}{(2\pi)^3} \delta(|\mathbf{k}| - k_{F,\eta}). \end{aligned} \quad (6)$$

Since  $\int \boldsymbol{\Omega}_{\eta} \cdot d\mathbf{S}_{\mathbf{k}} = 2\pi\eta = \pm 2\pi$ , the response current proves to be quantized with additional relaxation time. Assuming a monochromatic wave  $\mathbf{E}(t) = \text{Re}\{\mathbf{E}_0 e^{-i\omega_0 t}\}$  and going back to dimensional units, for second order conductivity tensor  $\sigma_{\alpha\beta\gamma}$  (we focus only on dc component of the response,  $j_{\alpha}(\omega_j = 0) = \sigma_{\alpha\beta\gamma}(0)E_{0\beta}E_{0\gamma}^*$ ), we arrive at

$$\sigma_{\alpha\beta\gamma}(0) = \varepsilon_{\alpha\beta\gamma} \frac{e^3}{24\pi^2\hbar^2} \sum_{\eta} \frac{\eta\tau_{\eta}(\mu_{\eta})}{1 - i\omega_0\tau_{\eta}(\mu_{\eta})}, \quad (7)$$

which is the main result of the present work. Eq. (7) allows for a particularly simple interpretation for the case

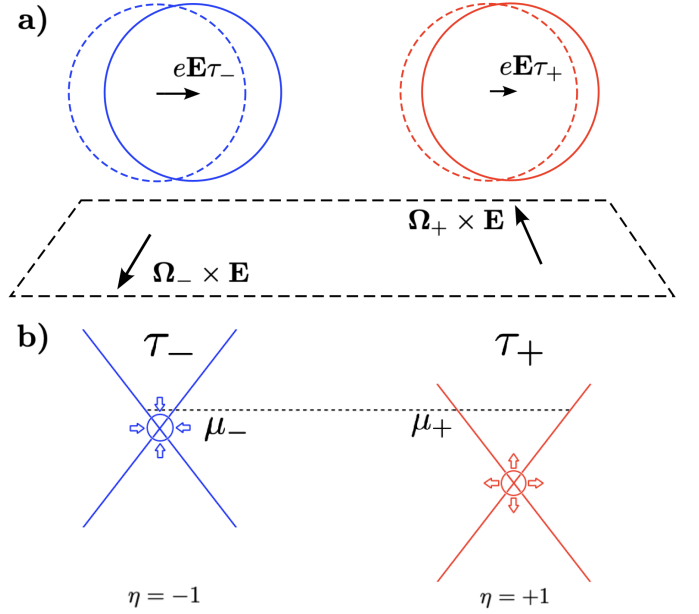


FIG. 1. Schematic illustration of the nonlinear Hall effect origin. a) Fermi surface shift is shown to be proportional to node-dependent momentum relaxation time  $\tau_+$ ,  $\tau_-$ . Anomalous Berry curvature velocities are shown to have opposite directions for opposite chirality nodes. b) 'Hot' and 'cold' Berry curvature monopoles that arise due to mirror symmetry breaking (either chiral anomaly induced or due to intrinsic symmetry breaking) are shown.

of low frequencies  $\omega_0\tau_\eta \ll 1$ . Namely, topological current is proportional to Berry curvature and node's chirality  $\eta$ . However, at the same time it accounts for the Fermi surface shift, which is proportional to the shortest timescale of the problem ( $\tau_\eta$ ). In the case of broken chiral symmetry, the overall contribution is non-vanishing and  $\sigma_{\alpha\beta\gamma}(0) \propto \tau_+ - \tau_-$ . This could be understood with the help of time-resolved Hall signal (see Fig. 4a). In the high frequency regimes, Fermi surface shift becomes frequency and not  $\tau_\eta$  dependent, thus effectively restoring chiral symmetry. Therefore, the nonlinear Hall current in Eq. (7) vanishes for  $\omega_0\tau_\eta \gg 1$ .

For short-ranged impurity scattering it was proven previously that  $\tau_\eta^{-1} \propto \nu(\mu_\eta) \propto \mu_\eta^2$  [26]. Therefore, in an extreme limit  $\mu_- \ll \mu_+$  one should have a truly Berry monopole contribution, provided that  $\tau_- \gg \tau_+$ .

The most general way to break chiral symmetry in mirror-symmetric systems is to apply parallel electric and magnetic field which would lead to the relative shift of different chirality nodes  $\mu_+ - \mu_-$  due to chiral anomaly effect (see also Fig. 1b). The value of the shift  $\mu_+ - \mu_-$  was previously predicted in [27–29] to be

$$\mu_+ - \mu_- = \frac{e^2 EB}{4\pi^2\hbar^2\nu_F} \tau_{\text{ch}}, \quad (8)$$

with  $\tau_{\text{ch}}$  being the internode chirality relaxation time. For materials with intrinsically broken mirror symmetry

[19–22] the response in Eq. (7) is finite even in the absence of electrical and magnetic fields.

Performing real material estimate for TaAs subject to  $B = 9\text{ T}$ ,  $E = 10^4\text{ V/m}$  and  $\tau \sim 10^{-13}\text{ s}$ ,  $\tau_{\text{ch}} \sim 10^{-11}\text{ s}$  (there is however a certain ambiguity in measuring chirality relaxation time due to the reasons mentioned in introduction) gives  $\sigma_{xyz} \sim 2 \cdot 10^{-4} \frac{A}{V^2}$ . Equivalently, comparing it with regular Drude current response  $j_D = e^2 \nu(\mu) v_F^2 \tau E / 3$ , we arrive at  $j_H / j_D \lesssim 5\%$ .

*Quantum approach using Landau level basis.* In this section, we perform a purely quantum Kubo formula computation for non-linear conductivity. This approach allows to treat electric and magnetic fields on equal footing. And as we show in what follows, it can be applied to both Dirac and Weyl semimetals unlike semiclassical calculation. The most general form of second order current response in Fourier representation reads

$$j_\alpha(\omega_j) = \int \frac{d\omega}{2\pi} \sigma_{\alpha\beta\gamma}(\omega, \omega_j - \omega) E^\beta(\omega) E^\gamma(\omega_j - \omega) \quad (9)$$

where  $\mathbf{E} = \text{Re} \{ \mathbf{E}_0 e^{-i\omega_0 t} \}$ .

In order to simplify second order response formula for  $\sigma_{\alpha\beta\gamma}(\omega_1, \omega_2)$  we switch to Matsubara representation (see also [30–32]):

$$\begin{aligned} \sigma_{\alpha\beta\gamma}(i\omega_1, i\omega_2) &= \frac{\chi_{\alpha\beta\gamma}(i\omega_1, i\omega_2) + \chi_{\beta\alpha\gamma}(i\omega_2, i\omega_1)}{\omega_1 \omega_2}, \\ \chi_{\alpha\beta\gamma}(i\omega_1, i\omega_2) &= \\ &= \frac{1}{V} \int \frac{d\varepsilon}{2\pi} \text{Tr} \left\langle \hat{j}_\alpha \hat{G}(i\varepsilon - i\omega_1) \hat{j}_\beta \hat{G}(i\varepsilon - i\omega_2) \hat{j}_\gamma \hat{G}(i\varepsilon) \right\rangle_{\text{dis}}, \end{aligned} \quad (10)$$

where  $\omega_j = \omega_1 + \omega_2$  and  $\langle \dots \rangle_{\text{dis}}$  is the disorder average. We assume that electronic properties are governed by a standard Weyl electron Hamiltonian in a magnetic field (described by vector potential  $\mathbf{A}$ )

$$\hat{H} = \eta v_F \boldsymbol{\sigma} \cdot \left( \mathbf{k} + \frac{e}{c} \mathbf{A} \right), \quad (11)$$

so that particle current  $\hat{j}_\alpha$  and Green function  $\hat{G}(i\varepsilon)$  are given by

$$\hat{j}_\alpha = e \partial_{k_\alpha} \hat{H} = \eta e \sigma_\alpha v_F, \quad \hat{G}(i\varepsilon) = (i\varepsilon - \hat{H})^{-1}. \quad (12)$$

Explicit computation of the non-linear response Eq.(10) in the basis of Landau levels depicted at Fig. 3 (see appendix A for details) leads to the same result as shown in Eq. (7). However, we would like to emphasize that Eq. (7) is justified only when interband optical transitions could be fully neglected (in the limit of  $\omega_0 \ll \mu_\eta$ ).

*Comparison with nonlinear Hall effects from other sources.* For a complete discussion of the result in Eq. (7), we compare it with previous relevant findings. It is known that based on its origin Hall effects could be conveniently separated into intrinsic, side jump and skew scattering parts. The result given by Eq. (6) is proportional to Berry curvature related anomalous velocity and

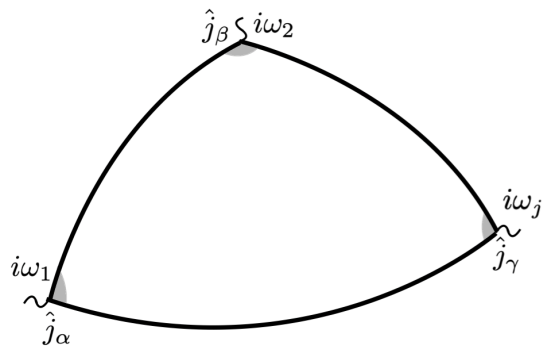


FIG. 2. Feynman diagram for a 3-point correlation function  $\chi_{\alpha\beta\gamma}(i\omega_1, i\omega_2)$ , with  $\omega_j = \omega_1 + \omega_2$ . Solid lines represent disorder-averaged Green function  $\langle \hat{G} \rangle$  from Eq. (10). Vertex corrections are shown by gray color.

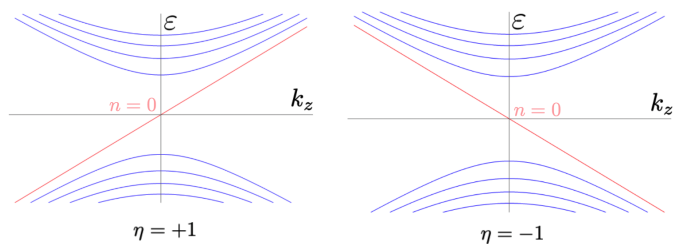


FIG. 3. Landau levels for both positive ( $\eta = 1$ ) and negative ( $\eta = -1$ ) chiralities Weyl nodes.  $k_z$  denotes longitudinal (with respect to  $\mathbf{B}$ ) momentum. ‘Chiral’ levels with linear dispersion are shown.

is evidently intrinsic. Hence, in what follows we compare it with other known intrinsic contributions [18, 25]. Nonetheless, it should be mentioned that other types of contributions (side jump and skew scattering) were thoroughly studied in [33, 34]. Namely, it was demonstrated that these effects, unlike our present result, rely on having a finite tilt velocity. Thus, we expect the results of [33] to be suppressed by  $u/v_F$ , where  $u$  is tilt velocity (such that for TaAs  $u/v_F \sim 0.1$ ).

As already mentioned in previous sections, a similar non-linear effect was predicted in [25] as a consequence of  $B$ -dependent part of Lorentz force combined with anomalous velocity contribution in tilted Weyl nodes. Although this effect is not chiral anomaly related and requires a lower power of  $E$  to hold ( $j_H \sim E^2 B$  while we predict  $j_H \sim E^3 B$ ), it appears to be proportional to the tilt velocity that is usually small. For real material TaAs [35, 36], order of magnitude estimate for  $E = 100\text{ V/cm}$ ,  $B = 9\text{ T}$  gives  $j_H / j_D \sim 1\%$  in [25] and  $j_H / j_D \lesssim 5\%$  for our prediction, proving that detecting of chiral anomaly related response is experimentally feasible in Weyl semimetals.

Another seminal work on this topic includes the so-called ‘Berry curvature dipole’ contribution [18]. This effect is the strongest near charge neutrality point. However, a relevant limit for the present study is for Fermi

level being high above in electron band, where the Berry curvature dipole decays rapidly and the two effects could thus be comparable. For instance, simulations performed for TaIrTe<sub>4</sub> compound [37] suggest that Berry curvature dipole could vanish for certain values of chemical potential. For Weyl semimetal with mirror symmetry, the Berry curvature dipole induced nonlinear Hall tensor in Eq. (7) is vanishing. Furthermore, both mechanisms discussed above [18, 25] heavily rely on the presence of finite tilting and vanish for untilted nodes. Our results are free from such an assumption, due to its monopole nature.

*Electron interaction and current quantization.* For interband transitions [38–40], de Juan et al. predicted that photocurrent is quantized as a function of frequency [38]. However, later it was later proven that the presence of interaction could remove the ideal quantization [30, 41]. Since the nonlinear Hall current in Eq. (7) is sensitive only to chirally asymmetric scattering channels, the proposed quantization is therefore more robust under electron interactions.

*Circular dichroism measurements.* Non-trivial Hall response discussed above could also manifest itself in optical measurements of circular dichroism [42–44]. For TR invariant systems with broken inversion symmetry, a homogeneous linear response is prohibited by Onsager symmetry relations [45]. In previous works [46, 47], consideration was mainly given to  $\mathbf{q}$ -linear contribution (with  $\mathbf{q}$  being the incident light wavevector). In contrast, here we would focus on non-linear part of the response instead. With the relation between conductivity and dielectric tensors

$$\varepsilon_{ij}(\omega_0, \mathbf{q}) = \delta_{ij} + \frac{4\pi i \sigma_{ij}(\omega_0, \mathbf{q})}{\omega_0} \quad (13)$$

and assuming that  $\mathbf{E} \parallel \mathbf{B} \parallel 0z$  and rotational symmetry in  $0xy$  plane, for  $\varepsilon_{ij}(\omega_0, \mathbf{q})$  we arrive at

$$\varepsilon_{ij}(\omega_0) = \begin{pmatrix} \varepsilon_{\perp}(\omega_0) & 4i\pi\sigma_{xy}(\omega_0)/\omega_0 & 0 \\ -4i\pi\sigma_{xy}(\omega_0)/\omega_0 & \varepsilon_{\perp}(\omega_0) & 0 \\ 0 & 0 & \varepsilon_{\parallel}(\omega_0) \end{pmatrix}. \quad (14)$$

Refraction indices for different modes are given by the eigenvalues of Eq. (14):  $n_{\parallel}^2 = \varepsilon_{\parallel}(\omega_0)$ ,  $n_{L(R)}^2 = \varepsilon_{\perp}(\omega_0) \pm 4\pi\sigma_{xy}/\omega_0$ . Chiral dichroism signal  $\gamma = \text{Im}(n_L - n_R)$  is then given by (also plotted in Fig. 4b for different magnetic field values)

$$\gamma_E \approx \frac{e^3}{6\pi\omega_0\hbar^2} E \sum_{\eta} \frac{\eta\tau_{\eta}}{1 + \omega_0^2\tau_{\eta}^2} \text{Re} \frac{1}{\sqrt{\varepsilon_{\perp}(\omega_0)}}. \quad (15)$$

The complete derivation of (15) could be found in appendix B. Now let us compare the finding in Eq. (15) with the previously known result for  $\mathbf{q}$ -linear contribution to circular dichroism signal [48]. Note that even though  $\gamma_E$  and  $\gamma_q$  pertain to different kind of response (dc vs ac response), it is still instructive to compare the

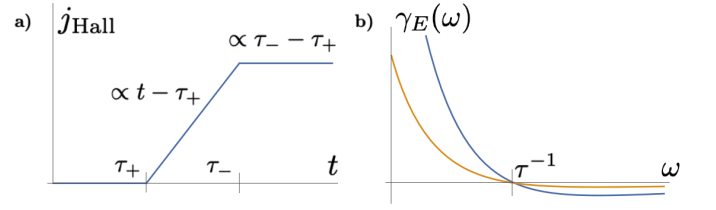


FIG. 4. a) Time-resolved Hall current.  $t < \tau_+$ : ballistic currents in both  $\eta = \pm 1$  nodes compensate each other.  $\tau_+ < t < \tau_-$ :  $\eta = +1$  current is saturated while  $\eta = -1$  is not.  $\tau_- < t$ : both  $\eta = \pm 1$  currents are saturated. b) Chiral dichroism signal  $\gamma_E$  due to non-linear Hall response. Blue line:  $(\tau_+ - \tau_-)/\tau_0 = 0.2$ , orange line:  $(\tau_+ - \tau_-)/\tau_0 = 0.15$ , with  $\tau_0$  being the momentum relaxation time for  $\mathbf{B} = 0$ .

magnitudes of the signals for future experimental tests. According to Ref. [48],  $\gamma_q$  reads

$$\gamma_q = \frac{4e^2}{3\pi\hbar^2c} \sum_{\eta} \eta\mu_{\eta}\tau_{\eta} \text{Re} \frac{1}{\sqrt{\varepsilon_{\perp}(\omega_0)}}, \quad (16)$$

so that  $\gamma_E \sim \frac{eEc}{\mu\omega_0} \gamma_q$  and for real material estimate (TaAs) ( $E = 100 \text{ V/cm}$ ,  $B = 9 \text{ T}$ ,  $\omega_0 = 10 \text{ THz}$ )  $\gamma_E/\gamma_q \sim 10$ . This in turn means that anomaly related chiral dichroism signal is easier to observe in dc response setup.

We now discuss the possible Fermi arc surface states contribution that inevitably arises due to topological Berry curvatures. In the limit of relatively large crystal volume, it is natural to expect surface contribution to be vanishingly small. Besides that, Weyl materials with few nodes could host a surface that does not support arc states [46]. We will leave the detailed study on surface contributions to future work.

*Dirac semimetal.* It is important to mention that, surprisingly, all of the above physics is applicable to the case of Dirac semimetals as well. Technically, it could be demonstrated with the help of Kubo formula calculation (see discussion in appendix A for details). The physical argument for that was previously developed in [29]. Namely, all of the chiral anomaly physics transfers to Dirac case if the bandgap  $\Delta_g$  is relatively small:  $\Delta_g \ll \varepsilon_F$ . The only difference is that the notion of chirality is replaced by helicity (which is a projection of particle's spin onto its momentum) and chirality relaxation time by helicity relaxation time. Real material estimate for Dirac semimetals ZrTe<sub>5</sub>, Na<sub>3</sub>Bi [8] gives  $j_H/j_D \sim 1\%$  already for  $B = 1 \text{ T}$ . Since chiral anomaly-nonrelated Berry curvature effects would cancel for Dirac case, this effect should be perfectly measurable.

To summarise, we predicted a non-vanishing Hall response in TR-invariant systems from Berry curvature monopole. We have demonstrated that chiral anomaly-induced relative shift of Weyl cones in energy space gives rise to chirally asymmetric intranode momentum relaxation times. Due to this inherent asymmetry, nonlinear Hall current is given by quantized monopole charge, weighted by node specific relaxation time. We further

discuss the corresponding nonlinear circular dichroism signal from the chiral asymmetry. The predicted effect is robust to interactions beyond simple impurity scattering, since only scattering channels which are chirally asymmetric would contribute to this effect.

*Acknowledgement.* We are grateful to Philip Moll and Liang Fu for helpful discussions. C.F. is supported by the Catalyst Fund of Canadian Institute for Advanced Research. Y. Z. is supported by the start-up fund at University of Tennessee Knoxville.

- 
- [1] H. B. Nielsen and M. Ninomiya, The adler-bell-jackiw anomaly and weyl fermions in a crystal, *Physics Letters B* **130**, 389 (1983).
- [2] X. Huang, L. Zhao, Y. Long, P. Wang, D. Chen, Z. Yang, H. Liang, M. Xue, H. Weng, Z. Fang, X. Dai, and G. Chen, Observation of the chiral-anomaly-induced negative magnetoresistance in 3d weyl semimetal taas, *Phys. Rev. X* **5**, 031023 (2015).
- [3] C. Shekhar, A. K. Nayak, Y. Sun, M. Schmidt, M. Nicklas, I. Leermakers, U. Zeitler, Y. Skourski, J. Wosnitza, Z. Liu, *et al.*, Extremely large magnetoresistance and ultrahigh mobility in the topological weyl semimetal candidate nbp, *Nature Physics* **11**, 645 (2015).
- [4] J. Du, H. Wang, Q. Chen, Q. Mao, R. Khan, B. Xu, Y. Zhou, Y. Zhang, J. Yang, B. Chen, *et al.*, Large unsaturated positive and negative magnetoresistance in weyl semimetal tap, *Science China Physics, Mechanics & Astronomy* **59**, 1 (2016).
- [5] Z. Wang, Y. Zheng, Z. Shen, Y. Lu, H. Fang, F. Sheng, Y. Zhou, X. Yang, Y. Li, C. Feng, and Z.-A. Xu, Helicity-protected ultrahigh mobility weyl fermions in nbp, *Phys. Rev. B* **93**, 121112 (2016).
- [6] C.-L. Zhang, S.-Y. Xu, I. Belopolski, Z. Yuan, Z. Lin, B. Tong, G. Bian, N. Alidoust, C.-C. Lee, S.-M. Huang, *et al.*, Signatures of the adler-bell-jackiw chiral anomaly in a weyl fermion semimetal, *Nature communications* **7**, 1 (2016).
- [7] H.-J. Kim, K.-S. Kim, J.-F. Wang, M. Sasaki, N. Satoh, A. Ohnishi, M. Kitaura, M. Yang, and L. Li, Dirac versus weyl fermions in topological insulators: Adler-bell-jackiw anomaly in transport phenomena, *Phys. Rev. Lett.* **111**, 246603 (2013).
- [8] J. Xiong, S. K. Kushwaha, T. Liang, J. W. Krizan, M. Hirschberger, W. Wang, R. J. Cava, and N. P. Ong, Evidence for the chiral anomaly in the dirac semimetal na<sub>3</sub>bi, *Science* **350**, 413 (2015).
- [9] C.-Z. Li, L.-X. Wang, H. Liu, J. Wang, Z.-M. Liao, and D.-P. Yu, Giant negative magnetoresistance induced by the chiral anomaly in individual cd<sub>3</sub>as<sub>2</sub> nanowires, *Nature communications* **6**, 10137 (2015).
- [10] T. Liang, Q. Gibson, M. N. Ali, M. Liu, R. Cava, and N. Ong, Ultrahigh mobility and giant magnetoresistance in the dirac semimetal cd<sub>3</sub>as<sub>2</sub>, *Nature materials* **14**, 280 (2015).
- [11] H. Li, H. He, H.-Z. Lu, H. Zhang, H. Liu, R. Ma, Z. Fan, S.-Q. Shen, and J. Wang, Negative magnetoresistance in dirac semimetal cd<sub>3</sub>as<sub>2</sub>, *Nature communications* **7**, 10301 (2016).
- [12] C. Zhang, E. Zhang, W. Wang, Y. Liu, Z.-G. Chen, S. Lu, S. Liang, J. Cao, X. Yuan, L. Tang, *et al.*, Room-temperature chiral charge pumping in dirac semimetals, *Nature communications* **8**, 13741 (2017).
- [13] Q. Li, D. E. Kharzeev, C. Zhang, Y. Huang, I. Pletikosić, A. Fedorov, R. Zhong, J. Schneeloch, G. Gu, and T. Valla, Chiral magnetic effect in zrte<sub>5</sub>, *Nature Physics* **12**, 550 (2016).
- [14] M. C. Steele, Anomalous longitudinal magnetoresistance of metal single crystals, *Phys. Rev.* **97**, 1720 (1955).
- [15] J. Babiskin, Oscillatory galvanomagnetic properties of bismuth single crystals in longitudinal magnetic fields, *Phys. Rev.* **107**, 981 (1957).
- [16] K. Yoshida, An anomalous behavior of the longitudinal magnetoresistance in semimetals, *Journal of the Physical Society of Japan* **41**, 574 (1976).
- [17] N. P. Armitage, E. J. Mele, and A. Vishwanath, Weyl and dirac semimetals in three-dimensional solids, *Rev. Mod. Phys.* **90**, 015001 (2018).
- [18] I. Sodemann and L. Fu, Quantum nonlinear hall effect induced by berry curvature dipole in time-reversal invariant materials, *Phys. Rev. Lett.* **115**, 216806 (2015).
- [19] F. De Juan, A. G. Grushin, T. Morimoto, and J. E. Moore, Quantized circular photogalvanic effect in weyl semimetals, *Nature communications* **8**, 15995 (2017).
- [20] D. Rees, K. Manna, B. Lu, T. Morimoto, H. Borrmann, C. Felser, J. Moore, D. H. Torchinsky, and J. Orenstein, Helicity-dependent photocurrents in the chiral weyl semimetal rhsi, *Science advances* **6**, eaba0509 (2020).
- [21] Z. Ni, K. Wang, Y. Zhang, O. Pozo, B. Xu, X. Han, K. Manna, J. Paglione, C. Felser, A. G. Grushin, *et al.*, Giant topological longitudinal circular photo-galvanic effect in the chiral multifold semimetal cosi, *Nature communications* **12**, 154 (2021).
- [22] E. Druke, R. Owen, M. Day, S. Tian, C. Li, H. Lei, S. Cundiff, and L. Zhao, Second order nonlinear responses in chiral weyl semimetal cosi, *Bulletin of the American Physical Society* **65** (2020).
- [23] Y. Zhang, Y. Sun, and B. Yan, Berry curvature dipole in weyl semimetal materials: an ab initio study, *Physical Review B* **97**, 041101 (2018).
- [24] Z. Du, C. Wang, H.-Z. Lu, and X. Xie, Band signatures for strong nonlinear hall effect in bilayer wte<sub>2</sub>, *Physical review letters* **121**, 266601 (2018).
- [25] R.-H. Li, O. G. Heinonen, A. A. Burkov, and S. S.-L. Zhang, Nonlinear hall effect in weyl semimetals induced by chiral anomaly, *Phys. Rev. B* **103**, 045105 (2021).
- [26] Y. Ominato and M. Koshino, Quantum transport in a three-dimensional weyl electron system, *Phys. Rev. B* **89**, 054202 (2014).
- [27] D. T. Son and B. Z. Spivak, Chiral anomaly and classical negative magnetoresistance of weyl metals, *Phys. Rev. B* **88**, 104412 (2013).
- [28] B. Z. Spivak and A. V. Andreev, Magnetotransport phenomena related to the chiral anomaly in weyl semimetals, *Phys. Rev. B* **93**, 085107 (2016).
- [29] A. Andreev and B. Spivak, Longitudinal negative magnetoresistance and magnetotransport phenomena in conventional and topological conductors, *Physical review letters* **120**, 026601 (2018).

- [30] A. Avdoshkin, V. Kozii, and J. E. Moore, Interactions remove the quantization of the chiral photocurrent at weyl points, *Phys. Rev. Lett.* **124**, 196603 (2020).
- [31] G. Bednik and V. Kozii, Magnetic field induces giant nonlinear optical response in weyl semimetals, arXiv preprint arXiv:2310.02578 (2023).
- [32] S. João and J. V. P. Lopes, Basis-independent spectral methods for non-linear optical response in arbitrary tight-binding models, *Journal of Physics: Condensed Matter* **32**, 125901 (2019).
- [33] Z. Du, C. Wang, S. Li, H.-Z. Lu, and X. Xie, Disorder-induced nonlinear hall effect with time-reversal symmetry, *Nature Communications* **10**, 3047 (2019).
- [34] Z. Du, C. Wang, H.-P. Sun, H.-Z. Lu, and X. Xie, Quantum theory of the nonlinear hall effect, *Nature communications* **12**, 5038 (2021).
- [35] B. Xu, Y. M. Dai, L. X. Zhao, K. Wang, R. Yang, W. Zhang, J. Y. Liu, H. Xiao, G. F. Chen, A. J. Taylor, D. A. Yarotski, R. P. Prasankumar, and X. G. Qiu, Optical spectroscopy of the weyl semimetal taas, *Phys. Rev. B* **93**, 121110 (2016).
- [36] B. Cheng, T. Schumann, S. Stemmer, and N. P. Armitage, Probing charge pumping and relaxation of the chiral anomaly in a dirac semimetal, *Science Advances* **7**, eabg0914 (2021).
- [37] D. Kumar, C.-H. Hsu, R. Sharma, T.-R. Chang, P. Yu, J. Wang, G. Eda, G. Liang, and H. Yang, Room-temperature nonlinear hall effect and wireless radiofrequency rectification in weyl semimetal tairte4, *Nature Nanotechnology* **16**, 421 (2021).
- [38] F. de Juan, Y. Zhang, T. Morimoto, Y. Sun, J. E. Moore, and A. G. Grushin, Difference frequency generation in topological semimetals, *Phys. Rev. Res.* **2**, 012017 (2020).
- [39] Y. Sun, Q. Xu, Y. Zhang, C. Le, and C. Felser, Optical method to detect the relationship between chirality of reciprocal space chiral multifold fermions and real space chiral crystals, *Phys. Rev. B* **102**, 104111 (2020).
- [40] Y. Zhang, H. Ishizuka, J. van den Brink, C. Felser, B. Yan, and N. Nagaosa, Photogalvanic effect in weyl semimetals from first principles, *Phys. Rev. B* **97**, 241118 (2018).
- [41] I. Mandal, Effect of interactions on the quantization of the chiral photocurrent for double-weyl semimetals, *Symmetry* **12**, 919 (2020).
- [42] S. Sekh and I. Mandal, Circular dichroism as a probe for topology in three-dimensional semimetals, *Phys. Rev. B* **105**, 235403 (2022).
- [43] I. Mandal, Signatures of two-and three-dimensional semimetals from circular dichroism, *International Journal of Modern Physics B* , 2450216 (2023).
- [44] A. R. Karmakar, S. Nandy, G. Das, and K. Saha, Probing mirror anomaly and classes of dirac semimetals with circular dichroism, *Physical Review Research* **3**, 013230 (2021).
- [45] Y. Tokura and N. Nagaosa, Nonreciprocal responses from non-centrosymmetric quantum materials, *Nature communications* **9**, 3740 (2018).
- [46] M. Kargarian, M. Randeria, and N. Trivedi, Theory of kerr and faraday rotations and linear dichroism in topological weyl semimetals, *Scientific reports* **5**, 12683 (2015).
- [47] J. Ahn and B. Ghosh, Topological circular dichroism in chiral multifold semimetals, *Phys. Rev. Lett.* **131**, 116603 (2023).
- [48] P. Hosur and X.-L. Qi, Tunable circular dichroism due to the chiral anomaly in weyl semimetals, *Phys. Rev. B* **91**, 081106 (2015).
- [49] A. Bharti, M. S. Mrudul, and G. Dixit, High-harmonic spectroscopy of light-driven nonlinear anisotropic anomalous hall effect in a weyl semimetal, *Phys. Rev. B* **105**, 155140 (2022).

## Appendix A: Non-linear Hall response $\sigma_{\alpha\beta\gamma}$ Kubo formula derivation

In this appendix, we explicitly derive the non-linear Hall response  $\sigma_{\alpha\beta\gamma}$  for both Weyl and Dirac semimetals with the help of diagram technique in the basis of Landau levels. As shown in the main text, the general second order response  $\sigma_{\alpha\beta\gamma}(i\omega_1, i\omega_2)$  is expressed through 3-point correlation functions  $\chi_{\alpha\beta\gamma}(i\omega_1, i\omega_2)$ :

$$\chi_{\alpha\beta\gamma}(i\omega_1, i\omega_2) = \int \frac{d\varepsilon}{2\pi} \text{Tr} \langle j_\alpha G(i\varepsilon - i\omega_1) j_\beta G(i\varepsilon - i\omega_2) j_\gamma G(i\varepsilon) \rangle_{\text{dis}}. \quad (\text{A1})$$

Since the scattering is treated perturbatively, introducing disorder would lead only to a substitute of bare Green function by an averaged one plus vertex corrections. Disorder-averaged Green function  $\langle \hat{G} \rangle$  of Weyl fermion for the case of finite magnetic field  $\mathbf{B} \parallel 0z$  in coordinate representation is given by

$$\begin{aligned} \langle \hat{G} \rangle(i\varepsilon, \mathbf{r}_1, \mathbf{r}_2) &= \sum_{n, k_x, k_z} \frac{|\Psi_{n, k_x, k_z}(\mathbf{r}_1)\rangle \langle \Psi_{n, k_x, k_z}(\mathbf{r}_2)|}{i\varepsilon - E_n(k_z) + \mu_\eta + \frac{i}{2\tau_\eta} \text{sgn}(E_n(k_z) - \mu_\eta)}, \\ E_n(k_z) &= \text{sgn}(n) v_F \sqrt{2|n|/l_B^2 + k_z^2}, \quad n \neq 0 \\ E_0(k_z) &= \eta v_F k_z, \end{aligned} \quad (\text{A2})$$

where  $\Psi_{n, k_x, k_z}$  and  $E_n(k_z)$  stand for eigenfunctions and eigenenergies of Eq. (11) (see also Fig. 3) enumerated by integer  $n$ ;  $k_z$  is longitudinal with respect to  $\mathbf{B}$  momentum,  $\mu_\eta, \tau'_\eta = \frac{2}{3}\tau_\eta$  are the chirality-dependent chemical potential

and scattering time correspondingly. In what follows we demonstrate that simple scattering time  $\tau'_\eta$  in Eq. (A2) differs from momentum relaxation time  $\tau_\eta$  used in semiclassical analysis of Eq. (3) only by numerical factor 2/3. It should be however noted that this relaxation times relation was proven previously in [29] for the case of linear response. We generalize this to non-linear case.

We proceed with explicitly evaluating 3-point correlation function with disorder averaged Green function with later showing that vertex corrections will only lead to replacing of scattering time  $\tau'_\eta$  by transport momentum relaxation time  $\tau_\eta$ . For analytical derivation present in this section we stick to the approach developed in [30, 31] but with an account for impurity scattering.

Employing Landau level representation for averaged over disorder Green function  $\langle G \rangle(i\varepsilon)$  given by Eq. (A2) and plugging it into Eq. (A1), we arrive at:

$$\chi_{\alpha\beta\gamma}(i\omega_1, i\omega_2) = \frac{eB}{2\pi\hbar c} \sum_{n_1, n_2, n_3} \int \frac{dk_z}{2\pi} \int \frac{d\varepsilon}{2\pi} \frac{Z_{\alpha\beta\gamma}^{n_1 n_2 n_3}}{\left(i\varepsilon - i\omega_1 - E_{n_2}(k_z) + \mu_\eta + \frac{i}{2\tau'_\eta} \text{sgn}(E_{n_2}(k_z) - \mu_\eta)\right)} \cdot \frac{1}{\left(i\varepsilon - i\omega_j - E_{n_3}(k_z) + \mu_\eta + \frac{i}{2\tau'_\eta} \text{sgn}(E_{n_3}(k_z) - \mu_\eta)\right) \left(i\varepsilon - E_{n_1}(k_z) + \mu_\eta + \frac{i}{2\tau'_\eta} \text{sgn}(E_{n_1}(k_z) - \mu_\eta)\right)},$$

$$Z_{\alpha\beta\gamma}^{n_1 n_2 n_3} = \langle n_1 | \hat{j}_\alpha | n_2 \rangle \langle n_2 | \hat{j}_\beta | n_3 \rangle \langle n_3 | \hat{j}_\gamma | n_1 \rangle, \quad (\text{A3})$$

where  $|n_{1,2,3}\rangle$  denote Landau level states. However, since the final result for nonlinear response Eq. (7) does not explicitly demonstrate magnetic field dependence, in what follows we would adopt semiclassical limit  $B \rightarrow 0$ . This in turn means that the sums in Eq. (A3) would be replaced by integrals over continuous momentum and the Green function  $\langle G \rangle(i\varepsilon)$  would be also taken in momentum representation:

$$\langle G \rangle(i\varepsilon, \mathbf{k}) = \frac{P_+(\mathbf{k})}{i\varepsilon - v_F k + \mu_\eta + \frac{i}{2\tau'_\eta} \text{sign}\varepsilon} + \frac{P_-(\mathbf{k})}{i\varepsilon + v_F k + \mu_\eta + \frac{i}{2\tau'_\eta} \text{sign}\varepsilon}, \quad P_\pm(\mathbf{k}) = \frac{1}{2} \left(1 \pm \boldsymbol{\sigma} \cdot \hat{\mathbf{k}}\right). \quad (\text{A4})$$

$\tau'_\eta(\mu_\eta)$  in (A4) is however  $B$ -dependent in a sense that  $\mu_+ \neq \mu_-$  due to chiral anomaly effect.

### 1. 3-point correlation function $\chi_{\alpha\beta\gamma}$ calculation

Since  $j_\alpha = \eta e v_F \sigma_\alpha$ , making use of Eq. (A1) and Eq. (A4), for  $\chi_{\alpha\beta\gamma}(i\omega_1, i\omega_2)$  we arrive at

$$\chi_{\alpha\beta\gamma}(i\omega_1, i\omega_2) = \eta e^3 v_F^3 \int \frac{d\varepsilon}{2\pi} \int \frac{d^3\mathbf{k}}{(2\pi)^3} \left[ \frac{\text{tr} \{ \sigma_\alpha P_-(\mathbf{k}) \sigma_\beta P_+(\mathbf{k}) \sigma_\gamma P_+(\mathbf{k}) \}}{\left(i\varepsilon - i\omega_1 + \mu + v_F k + \frac{i}{2\tau'_\eta} \text{sign}(\varepsilon - \omega_1)\right) \left(i\varepsilon - i\omega_j - v_F k + \mu + \frac{i}{2\tau'_\eta} \text{sign}(\varepsilon - \omega_j)\right) \left(i\varepsilon - v_F k + \mu + \frac{i}{2\tau'_\eta} \text{sign}\varepsilon\right)} + \frac{\text{tr} \{ \sigma_\alpha P_+(\mathbf{k}) \sigma_\beta P_-(\mathbf{k}) \sigma_\gamma P_-(\mathbf{k}) \}}{\left(i\varepsilon - i\omega_1 - v_F k + \mu + \frac{i}{2\tau'_\eta} \text{sign}(\varepsilon - \omega_1)\right) \left(i\varepsilon - i\omega_j + v_F k + \mu + \frac{i}{2\tau'_\eta} \text{sign}(\varepsilon - \omega_j)\right) \left(i\varepsilon + v_F k + \mu + \frac{i}{2\tau'_\eta} \text{sign}\varepsilon\right)} + \frac{\text{tr} \{ \sigma_\alpha P_+(\mathbf{k}) \sigma_\beta P_+(\mathbf{k}) \sigma_\gamma P_-(\mathbf{k}) \}}{\left(i\varepsilon - i\omega_1 - v_F k + \mu + \frac{i}{2\tau'_\eta} \text{sign}(\varepsilon - \omega_1)\right) \left(i\varepsilon - i\omega_j - v_F k + \mu + \frac{i}{2\tau'_\eta} \text{sign}(\varepsilon - \omega_j)\right) \left(i\varepsilon + v_F k + \mu + \frac{i}{2\tau'_\eta} \text{sign}\varepsilon\right)} + \frac{\text{tr} \{ \sigma_\alpha P_-(\mathbf{k}) \sigma_\beta P_-(\mathbf{k}) \sigma_\gamma P_+(\mathbf{k}) \}}{\left(i\varepsilon - i\omega_1 + v_F k + \mu + \frac{i}{2\tau'_\eta} \text{sign}(\varepsilon - \omega_1)\right) \left(i\varepsilon - i\omega_j + v_F k + \mu + \frac{i}{2\tau'_\eta} \text{sign}(\varepsilon - \omega_j)\right) \left(i\varepsilon - v_F k + \mu + \frac{i}{2\tau'_\eta} \text{sign}\varepsilon\right)} + \frac{\text{tr} \{ \sigma_\alpha P_+(\mathbf{k}) \sigma_\beta P_-(\mathbf{k}) \sigma_\gamma P_+(\mathbf{k}) \}}{\left(i\varepsilon - i\omega_1 - v_F k + \mu + \frac{i}{2\tau'_\eta} \text{sign}(\varepsilon - \omega_1)\right) \left(i\varepsilon - i\omega_j + v_F k + \mu + \frac{i}{2\tau'_\eta} \text{sign}(\varepsilon - \omega_j)\right) \left(i\varepsilon - v_F k + \mu + \frac{i}{2\tau'_\eta} \text{sign}\varepsilon\right)} + \frac{\text{tr} \{ \sigma_\alpha P_-(\mathbf{k}) \sigma_\beta P_+(\mathbf{k}) \sigma_\gamma P_-(\mathbf{k}) \}}{\left(i\varepsilon - i\omega_1 + v_F k + \mu + \frac{i}{2\tau'_\eta} \text{sign}(\varepsilon - \omega_1)\right) \left(i\varepsilon - i\omega_j - v_F k + \mu + \frac{i}{2\tau'_\eta} \text{sign}(\varepsilon - \omega_j)\right) \left(i\varepsilon + v_F k + \mu + \frac{i}{2\tau'_\eta} \text{sign}\varepsilon\right)} \right], \quad (\text{A5})$$

where  $\omega_j = \omega_1 + \omega_2$ , the sum over Landau level index  $n$  is replaced by integration over semiclassical momentum  $\mathbf{k}$  and  $\text{tr} \{ \dots \}$  stands for the trace over spin degrees of freedom. In what follows we switch to integration in spherical



coordinates of  $\mathbf{k}$ :  $\int \frac{d^3\mathbf{k}}{(2\pi)^3} = \int_0^\infty \nu(\varepsilon)d\varepsilon \int \frac{d\Omega_{\mathbf{k}}}{4\pi}$ ,  $\varepsilon = v_F|\mathbf{k}|$ . As for angle integration, a straightforward calculation suggests that

$$\langle \text{tr} \{ \sigma_\alpha P_+(\mathbf{k}) \sigma_\beta P_+(\mathbf{k}) \sigma_\gamma P_-(\mathbf{k}) \} \rangle_{\hat{\mathbf{k}}} = \langle \text{tr} \{ \sigma_\alpha P_+(\mathbf{k}) \sigma_\beta P_-(\mathbf{k}) \sigma_\gamma P_-(\mathbf{k}) \} \rangle_{\hat{\mathbf{k}}} = \frac{1}{3} i \varepsilon_{\alpha\beta\gamma}, \quad (\text{A6})$$

where  $\langle \dots \rangle_{\hat{\mathbf{k}}}$  stands for angular average over momentum directions. Thus, according to Eq. (A6), all traces appearing in (A5) are identical which allows to effectively extend the integration over  $\varepsilon$  to the whole real axis by grouping 2 subsequent terms into one contribution. Assuming the limit  $\omega_{1,2} \ll \mu$  (which is equivalent to neglecting all vertical optical transitions), we then arrive at

$$\begin{aligned} \chi_{\alpha\beta\gamma}(i\omega_1, i\omega_2) = & \\ = \frac{1}{3} \varepsilon_{\alpha\beta\gamma} \eta e^3 v_F^3 \nu_F \int d\varepsilon & \left[ \frac{\theta(\varepsilon) - \theta(\varepsilon - \omega_j)}{\left( 2i\varepsilon - i\omega_1 + 2\mu + \frac{i}{2\tau'_\eta} (\text{sign}(\varepsilon - \omega_1) + \text{sign}(\varepsilon)) \right) \left( -i\omega_j + \frac{i}{2\tau'_\eta} (\text{sign}(\varepsilon - \omega_j) - \text{sign}(\varepsilon)) \right)} + \right. \\ & + \frac{\theta(\varepsilon - \omega_1) - \theta(\varepsilon - \omega_j)}{\left( 2i\varepsilon - i\omega_1 + 2\mu + \frac{i}{2\tau'_\eta} (\text{sign}(\varepsilon + \text{sign}(\varepsilon - \omega_1))) \right) \left( -i\omega_j + i\omega_1 + \frac{i}{2\tau'_\eta} (\text{sign}(\varepsilon - \omega_j) - \text{sign}(\varepsilon - \omega_1)) \right)} \\ & \left. + \frac{\theta(\varepsilon) - \theta(\varepsilon - \omega_1)}{\left( -i\omega_1 + \frac{i}{2\tau'_\eta} (\text{sign}(\varepsilon - \omega_1) - \text{sign}(\varepsilon)) \right) \left( 2i\varepsilon - i\omega_j + 2\mu + \frac{i}{2\tau'_\eta} (\text{sign}(\varepsilon - \omega_j) + \text{sign}(\varepsilon)) \right)} \right] \quad (\text{A7}) \end{aligned}$$

Assuming for the sake of simplicity that  $\omega_1 > 0$  and performing integration over  $\varepsilon$ , we have

$$\chi_{\alpha\beta\gamma}(i\omega_1, i\omega_2) \approx \eta e^3 v_F^3 \nu_F \frac{1}{3} \varepsilon_{\alpha\beta\gamma} \left[ \frac{\omega_j}{2\mu(-i\omega_j - i/\tau'_\eta)} + \frac{\omega_2}{2\mu(-i\omega_2 - i/\tau'_\eta)} + \frac{\omega_1}{2\mu(-i\omega_1 - i/\tau'_\eta)} \right] \quad (\text{A8})$$

However, it is evident that in the leading approximation in  $\omega_{1,2}/\mu$  the expression  $\chi_{\alpha\beta\gamma}(i\omega_1, i\omega_2) - \chi_{\alpha\beta\gamma}(i\omega_2, i\omega_1)$  vanishes. Therefore, one should take into account correction terms, keeping in mind the limit  $\omega_1 + \omega_2 \rightarrow 0$  and expanding over  $\omega_{1,2}/\mu$ :

$$\chi_{\alpha\beta\gamma}(i\omega_1, i\omega_2) \approx \eta e^3 v_F^3 \nu_F \frac{1}{3} \varepsilon_{\alpha\beta\gamma} \left[ \frac{\omega_j}{2\mu(-i\omega_j - i/\tau'_\eta)} + \frac{\omega_2}{2\mu(-i\omega_2 - i/\tau'_\eta)} + \frac{\omega_1}{2\mu(-i\omega_1 - i/\tau'_\eta)} + \frac{\omega_1^2}{4\mu^2(\omega_1 + 1/\tau'_\eta)} \right] \quad (\text{A9})$$

For  $\chi_{\alpha\beta\gamma}(i\omega_2, i\omega_1)$  we have

$$\chi^{\alpha\beta\gamma}(i\omega_2, i\omega_1) \approx \eta e^3 v_F^3 \nu_F \frac{1}{3} \varepsilon_{\alpha\beta\gamma} \left[ \frac{\omega_j}{2\mu(-i\omega_j - i/\tau'_\eta)} + \frac{\omega_2}{2\mu(-i\omega_2 - i/\tau'_\eta)} + \frac{\omega_1}{2\mu(-i\omega_1 - i/\tau'_\eta)} - \frac{\omega_1^2}{4\mu^2(\omega_1 + 1/\tau'_\eta)} \right] \quad (\text{A10})$$

so that for the chiral one node contribution we arrive at

$$\sigma_{\alpha\beta\gamma} = \varepsilon_{\alpha\beta\gamma} \frac{1}{\omega^2} \eta e^3 v_F^3 \nu_F \frac{1}{3} \frac{\omega^2}{2\mu^2(-i\omega + 1/\tau'_\eta)} = \varepsilon_{\alpha\beta\gamma} \frac{1}{\omega^2} \eta e^3 v_F^3 \frac{\mu^2}{2\pi^2 v_F^3} \frac{1}{3} \frac{\omega^2}{2\mu^2(-i\omega + 1/\tau'_\eta)} \rightarrow \varepsilon_{\alpha\beta\gamma} \eta \frac{e^3}{12\pi^2} \frac{\tau'_\eta}{1 - i\omega\tau'_\eta}. \quad (\text{A11})$$

Thus, net nonlinear response reads (in full agreement with semiclassical result Eq. (7))

$$\sigma_{\alpha\beta\gamma} = \varepsilon_{\alpha\beta\gamma} \frac{e^3}{12\hbar^2\pi^2} \sum_{\eta} \frac{\eta\tau'_\eta}{1 - i\omega\tau'_\eta}, \quad (\text{A12})$$

where  $\eta$  stands for chirality. Note that extra factor of 2 arises due to different (again, by factor of 2) definitions of  $\sigma_{\alpha\beta\gamma}$  in Eqs. (7) and (9).

## 2. Vertex corrections

Taking into account vertex corrections leads to the replacement of scattering time by transport momentum relaxation time. Since for Gaussian disorder in Weyl semimetals  $\langle V(\mathbf{r})V(\mathbf{r}') \rangle = n_{\text{imp}} V^2 \delta(\mathbf{r} - \mathbf{r}') = \frac{1}{\pi\nu_F\tau'_\eta} \delta(\mathbf{r} - \mathbf{r}')$ , one ladder step contribution is given by

$$\frac{1}{\pi\nu_F\tau'_\eta} \int \frac{d^3\mathbf{q}}{(2\pi)^3} \hat{G}(i\varepsilon - i\omega, \mathbf{q}) \hat{j}_\alpha \hat{G}(i\varepsilon, \mathbf{q}) = \frac{1}{\pi\nu_F\tau'_\eta} \int_0^\infty \nu(\xi_{\mathbf{q}}) d\xi_{\mathbf{q}} \int \frac{d\mathbf{n}_{\mathbf{q}}}{4\pi} \hat{G}(i\varepsilon - i\omega, \mathbf{q}) \hat{j}_\alpha \hat{G}(i\varepsilon, \mathbf{q}), \quad (\text{A13})$$



where  $\xi_{\mathbf{q}} = v_F |\mathbf{q}|$ . Plugging Eq. (A4) into Eq. (A13), we arrive at

$$\begin{aligned}
& \frac{1}{\pi \nu_F \tau'_\eta} \int_0^\infty \nu(\xi_{\mathbf{q}}) d\xi_{\mathbf{q}} \int \frac{d\mathbf{n}_{\mathbf{q}}}{4\pi} \frac{P_+(\mathbf{n}_{\mathbf{q}}) \hat{j}_\alpha P_+(\mathbf{n}_{\mathbf{q}})}{(i\varepsilon - i\omega - v_F q + \mu_\eta + \frac{i}{2\tau'_\eta} \text{sign}(\varepsilon - \omega))(i\varepsilon - v_F q + \mu_\eta + \frac{i}{2\tau'_\eta} \text{sign}\varepsilon)} + \\
& + \frac{1}{\pi \nu_F \tau'_\eta} \int_0^\infty \nu(\xi_{\mathbf{q}}) d\xi_{\mathbf{q}} \int \frac{d\mathbf{n}_{\mathbf{q}}}{4\pi} \frac{P_-(\mathbf{n}_{\mathbf{q}}) \hat{j}_\alpha P_-(\mathbf{n}_{\mathbf{q}})}{(i\varepsilon - i\omega + v_F q + \mu_\eta + \frac{i}{2\tau'_\eta} \text{sign}(\varepsilon - \omega))(i\varepsilon + v_F q + \mu_\eta + \frac{i}{2\tau'_\eta} \text{sign}\varepsilon)} + \\
& + \frac{1}{\pi \nu_F \tau'_\eta} \int_0^\infty \nu(\xi_{\mathbf{q}}) d\xi_{\mathbf{q}} \int \frac{d\mathbf{n}_{\mathbf{q}}}{4\pi} \frac{P_+(\mathbf{n}_{\mathbf{q}}) \hat{j}_\alpha P_-(\mathbf{n}_{\mathbf{q}})}{(i\varepsilon - i\omega - v_F q + \mu_\eta + \frac{i}{2\tau'_\eta} \text{sign}(\varepsilon - \omega))(i\varepsilon + v_F q + \mu_\eta + \frac{i}{2\tau'_\eta} \text{sign}\varepsilon)} + \\
& + \frac{1}{\pi \nu_F \tau'_\eta} \int_0^\infty \nu(\xi_{\mathbf{q}}) d\xi_{\mathbf{q}} \int \frac{d\mathbf{n}_{\mathbf{q}}}{4\pi} \frac{P_-(\mathbf{n}_{\mathbf{q}}) \hat{j}_\alpha P_+(\mathbf{n}_{\mathbf{q}})}{(i\varepsilon - i\omega + v_F q + \mu_\eta + \frac{i}{2\tau'_\eta} \text{sign}(\varepsilon - \omega))(i\varepsilon - v_F q + \mu_\eta + \frac{i}{2\tau'_\eta} \text{sign}\varepsilon)} \quad (\text{A14})
\end{aligned}$$

Note however that the last two terms in Eq. (A14) would be suppressed by small parameter  $\omega/\mu \ll 1$  and could therefore be omitted. Employing the identity

$$\int \frac{d\mathbf{n}_{\mathbf{q}}}{4\pi} P_\pm(\mathbf{n}_{\mathbf{q}}) \sigma_\alpha P_\pm(\mathbf{n}_{\mathbf{q}}) = \frac{1}{4} \int \frac{d\mathbf{n}_{\mathbf{q}}}{4\pi} (\sigma_\alpha + \sigma_\beta n_\beta \sigma_\alpha \sigma_\gamma n_\gamma) = \frac{1}{6} \sigma_\alpha \quad (\text{A15})$$

and extending the integration in Eq. (A14) to negative half axis of  $\xi_{\mathbf{q}}$  in a way it was done in preceding section, for one ladder step contribution we arrive at

$$2 \cdot \frac{1}{6} \sigma_\alpha \frac{(\theta(\varepsilon) - \theta(\varepsilon - \omega)) i/\tau'_\eta}{i\omega + i/\tau'_\eta} = \frac{1}{3} \sigma_\alpha (\theta(\varepsilon) - \theta(\varepsilon - \omega)) \frac{1/\tau'_\eta}{1/\tau'_\eta + \omega} \quad (\text{A16})$$

so that, after summing up the series, vertex correction factor  $\Gamma(\omega)$  takes the form

$$\Gamma(\omega) = \hat{j}_\alpha \left( 1 + \frac{\frac{1}{3} \frac{1/\tau'_\eta}{1/\tau'_\eta - i\omega}}{1 - \frac{1}{3} \frac{1/\tau'_\eta}{1/\tau'_\eta - i\omega}} (\theta(\varepsilon) - \theta(\varepsilon - \omega)) \right). \quad (\text{A17})$$

Accounting for Eq. (A17) leads to replacing of scattering time  $\tau'_\eta$  in Eq. (A9) by transport time  $\tau_\eta$ .

### 3. Dirac case

Let us also note that the above calculation could be easily generalized for Dirac semimetals case. The reason is that Dirac node is actually comprised of two Weyl nodes with opposite chirality residing at the same momentum. Therefore, the Hamiltonian and Green function of a Dirac fermion read

$$\hat{H}_D = v_F \tau_3 \boldsymbol{\sigma} \cdot \mathbf{k}, \quad \hat{G}_D(\varepsilon) = \begin{pmatrix} (\varepsilon - v_F \boldsymbol{\sigma} \cdot \mathbf{k})^{-1} & 0 \\ 0 & (\varepsilon + v_F \boldsymbol{\sigma} \cdot \mathbf{k})^{-1} \end{pmatrix}, \quad \hat{\mathbf{j}} = v_F \begin{pmatrix} \boldsymbol{\sigma} & 0 \\ 0 & -\boldsymbol{\sigma} \end{pmatrix} \quad (\text{A18})$$

Since matrices in Eq. (A18) are diagonal, the result Eq. (7) transfers to Dirac case as well.

### Appendix B: Nonlinear circular dichroism derivation

Nonlinear circular dichroism signal  $\gamma = \text{Im}(n_L - n_R)$  is given by

$$\gamma = \text{Im} \left\{ \sqrt{\varepsilon_\perp(\omega_0) + \frac{4\pi i \sigma_{xy}}{\omega_0}} - \sqrt{\varepsilon_\perp(\omega_0) - \frac{4\pi i \sigma_{xy}}{\omega_0}} \right\}, \quad (\text{B1})$$

where

$$\sigma_{xy} = \frac{e^3}{24\pi^2 \hbar^2} E_z \sum_\eta \frac{\eta \tau_\eta}{1 - i\omega_0 \tau_\eta}$$

describes non-linear Hall conductivity. Assuming that  $\sigma_{xy} \ll \omega_0$  (which in case of TaAs corresponds to THz frequencies and gives the same estimate as  $\omega_0 > \omega_p$  condition for non-decaying EM wave) and performing Taylor expansion of (B1), we arrive at

$$\gamma = \frac{e^3}{6\pi\hbar^2\omega_0} E_z \sum_{\eta} \frac{\eta\tau_{\eta}}{1 + \omega_0^2\tau_{\eta}^2} \operatorname{Re} \frac{1}{\sqrt{\varepsilon_{\perp}(\omega_0)}} \quad (\text{B2})$$


---